Ultraviolet Jets and Bright Points in the Solar Chromosphere. I. Search for One-to-One Relationships

J.W. Cook
E.O. Hulburt Center for Space Research, Code 7668, Naval Research Laboratory, Washington, DC 20375-5352

R.J. Rutten
Sterrekundig Instituut, Postbus 80 000, NL–3508 TA Utrecht, The Netherlands

and

N.M. Hoekzema
Sterrekundig Instituut, Postbus 80 000, NL–3508 TA, Utrecht, The Netherlands

Received _____; accepted _____

ABSTRACT

Ultraviolet spectrograms and spectroheliograms of the solar chromosphere are used to test the suggestion (Dere et al. 1986, Rutten & Uitenbroek 1991a) that bright points observed at $\lambda = 1600\,\text{Å}$, chromospheric jets observed in C I lines near $\lambda = 1560\,\text{Å}$, and Ca II K_{2V} bright points are associated with each other and that they are all manifestations of the same wave interaction in the non-magnetic chromosphere. We search for spatio-temporal connections between 1600 Å bright points and C I blue jets using data from the HRTS VI rocket mission, comparing 1600 Å spectroheliograms and a co-spatial C I Dopplershift map on a pixel-by-pixel basis. We find no direct evidence for spatial co-location of bright points and jets, not for instantaneous correspondence and also not when allowing for phase delays as long as three minutes. Also, the average brightness evolution and its rms fluctuation are not obviously different between sites of large C I blueshift and the remaining surface.

Subject headings: Sun: granulation — Sun: oscillations — Sun: chromosphere

1. Introduction

Spectroheliograms from the HRTS experiment covering a passband near $\lambda = 1600$ Å (Cook et al. 1983, Cook & Ewing 1990, 1991) and similar filtergraph images taken with the Transition Region Camera (Bonnet et al. 1982, Foing & Bonnet 1984) have mapped solar emission in a wavelength band where it arises primarily from the solar temperature minimum region. These images show quiet areas to be structured by the magnetic network, the latter outlined by clusters of closely packed bright points of arcsecond size that are long lived, at least relative to the duration of a five-minute rocket flight. In addition, there are bright points within the internetwork areas or "cell interiors". They have similar size but evolve more rapidly, with characteristic lifetimes of about a minute. Whereas the network bright points are highly correlated with the absolute value of the magnetic flux density observed in photospheric magnetograms (Cook & Ewing 1990), it is not known whether the internetwork bright points are similarly associated with the low-level concentrations of magnetic flux presumably present in internetwork areas.

The 1600 Å internetwork bright points have often been assumed to be identical to the comparable Ca II K_{2V} grains because of their general morphological similarity (e.g., Bonnet et al. 1982, Cook et al. 1983, Foing & Bonnet 1984, Dere et al. 1986). The latter are internetwork bright points observed in a narrow band just blueward of the centers of the Ca II H & K lines. A magnetic origin has been claimed for these (Sivaraman & Livingston 1982), but in their review of the extensive K_{2V} literature Rutten & Uitenbroek (1991a) concluded that K_{2V} grains are of non-magnetic hydrodynamical origin, with much pattern interference between different wave modes including vertical velocity oscillations that produce 5–10 km s^{-1} sawtooth-shaped shifts of Ca II K_3 line center. Rutten & Uitenbroek (1991b) suggested a scenario in which K_{2V} grains mark moments and sites where backfalling matter from a previous shock passage falls onto the next upcoming shock front, after a well-developed wave train has gone through sufficient cycles. The recent numerical simulations of Carlsson & Stein (1994) quantify this scenario in detail (cf. reviews by Rutten 1994, 1995). A direct connection between K_{2V} and 1600 Å bright points is plausible, but so far, no Ca II H & K images of sufficient quality have been obtained simultaneously with 1600 Å images to establish such a relationship.

A separate 1600 Å phenomenon called "chromospheric jets" has been described by Dere et al. (1983) and is also discussed in Dere et al. (1984, 1986). These jets are small sites, of roughly one arcsec extent, where the lines of the C I multiplet near 1561 Å show bright, non-reversed emission peaks that are Dopplershifted over 10–20 km s^{-1}, predominantly to the blue. Such Dopplershifts are large for the low chromosphere, and much larger than both the error in the standard of rest (based on narrow emission lines of Si I) and the

typical measurement error per profile. Note that these jets differ from the higher-velocity "explosive events" seen in C IV lines from higher layers (cf. Dere et al. 1991, Dere 1994 and references therein). Jets occur primarily in internetwork areas; their average jet lifetime is around 40 s. At first, Dere et al. (1983) interpreted these jets as disk representations of off-limb white light spicules, but Dere et al. (1986) suggested instead that they are aspects of the same phenomenon which produces internetwork 1600 Å bright points and, presumably, Ca II K_{2V} grains. Rutten & Uitenbroek (1991a, 1991b) then speculated that if this is the case, the jets should represent the Ca II K_3 oscillation at another height and phase, so that spatio-temporal correlations should exist between C I jets and 1600 Å bright points when phase delays up to a few minutes are admitted.

In this paper, we search for such time-lagged correlations on a pixel-by-pixel basis but do not find clear evidence for such a relationship. In a companion paper (Hoekzema et al. 1996) we turn to statistical methods averaging over many pixels; weak but significant relationships then emerge.

2. Instrument and observations

The NRL High Resolution Telescope and Spectrograph (HRTS) has flown eight times as a sounding rocket experiment, and also on the Spacelab 2 mission onboard the Space Shuttle. In this paper we analyze data from the HRTS VI rocket flight above White Sands on 1988 November 20.

The basic HRTS instrument has been described by Brueckner et al. (1978) and Brueckner & Bartoe (1983). HRTS VI consisted of a 30 cm Cassegrain telescope which fed a stigmatic tandem-Wadsworth slit spectrograph (Bartoe & Brueckner 1975) covering a wavelength range of 1520–1580 Å, a broadband slit-jaw spectroheliograph tuned to a 10 Å wide passband centered at 1600 Å, and an Hα slit-jaw imager. The solar target area included quiet regions, a coronal hole, and several small active regions without sunspots. It was imaged with the broadband spectroheliograph and scanned with the spectrograph by stepping the slit transversely across the image. Both the spectroheliograph images and the spectra were registered on film and digitized later with a densitometer.

The observing program and the data have been described by Dere et al. (1989, 1991) in the context of coronal holes and explosive events. In this paper, we use seven sequential 1600 Å images and a co-spatial Dopplershift map obtained from the spectrograph data for a selected area near disk center.

2.1. The 1600 Å images

The broadband spectroheliograph produced an image of approximately 7.5×15 arcmin^2 field size from a reflection off the spectrograph slit. According to standard modeling of the solar atmosphere (Vernazza et al. 1981), 70% of the flux in its 10 Å passband around 1600 Å arises from the solar temperature minimum region with the remainder contributed by chromospheric emission lines within the passband. Images of various exposure were obtained during the HRTS VI flight; we use the 7.2 s exposures here because these show internetwork structure best. There are eight such exposures covering the area of interest scanned by the spectrograph slit, respectively taken at 90 s, 199 s, 221 s, 242 s, 274s, 295 s, 335 s, and 357 s after the moment of the HRTS VI launch. The first exposure is from early in the flight; the pointing was later changed before the spectrograph raster sequences were executed that are analyzed here. We have therefore not used this initial exposure except for visual inspections. The intervals between the remaining images are about 22 s, except after the fourth and sixth, when a change of pointing was made to start a new spectrograph raster sequence. The image taken at 221 s is shown in the top panel of Fig. 1. A subfield of all seven images is shown in Fig. 3.

The 1600 Å images were calibrated following Cook & Ewing (1990). The microdensitometer output was converted into relative intensities using the film characteristic curve and the average intensity in each image was then set to 150 ergs cm^{-2} s^{-1} Å^{-1} sr^{-1}, corresponding to a disk center continuum intensity at 1600 Å of 170 ergs cm^{-2} s^{-1} Å^{-1} sr^{-1} (Cook et al. 1980) and a center-to-limb ratio of 0.885 (Samain 1979) for the viewing angle of the center of the area studied below ($\cos\theta = \mu = 0.836$). Each intensity value in the images was then converted to brightness temperature. The error in this calibration is approximately (+67; -92) K in brightness temperature. However, for the present study the differential excursions from the average brightness temperature per spatial position are more important. For these, the primary error source is the inherent noise from film grain, which is less than 20 K in brightness temperature.

2.2. The spectrograph maps

The length of the spectrograph slit was 920 arcsec, approximately a solar radius. The slit was widened from its usual 0.5 arcsec width to 1.0 arcsec in order to increase the speed of the spectrograph and scan as large an area as possible during the short flight, at the cost of spectral resolution ($\Delta\lambda = 0.10$ Å). The slit was stepped across the target area in four raster sequences (shown in Fig. 1 of Dere et al. 1989). The first is separated from the other three by 2 arcmin and is not used in this paper. The other three sequences are adjacent;

together, they cover an area of 920 arcsec along the slit by 107 arcsec in the stepping direction. In the first raster, the slit was stepped over 50 arcsec in 26 steps of 2 arcsec; the second covered 20 arcsec in 21 steps of 1 arcsec; the third covered 40 arcsec in 21 steps of 2 arcsec width. From these, geometrically correct maps were produced by applying small corrections for actual slit positions and for the small gaps between the sequences.

The spectrograms cover the 1520 – 1580 Å wavelength range and contain the Si II 1526 Å and 1533 Å lines, the C IV 1548 Å and 1550 Å lines, and the C I multiplet near 1560 Å. After scanning, the digitized spectra were converted to absolute intensity using the film characteristic curve and a comparison between the relative intensities so obtained with absolute intensities from previous HRTS calibrations. The accuracy of the absolute calibration is not critical to the analysis reported here.

Following standard HRTS reduction procedures (Dere et al. 1984), maps of the intensity and velocity from a spectral line were constructed for the area covered by the raster sequences by measuring the zeroth moment (line intensity) and the first moment (average position) of a spectral line profile for each spatial resolution element along the slit for each slit position. The areas between raster steps are filled in through an interpolation scheme. This procedure requires relative intensity calibration only. The wavelength scale for converting first moments into Dopplershifts is obtained from the narrow Si I lines within the spectral range.

For the present analysis we have produced intensity and Dopplershift maps for the C I multiplet near 1560 Å by summing the intensities and averaging the Dopplershifts of the two composite C I profiles at 1560.7 Å and 1561.4 Å. The statistical Dopplershift measurement error has been estimated by Dere et al. (1984) to be about 2 km s^{-1}. However, there are several possible systematic errors. The C I multiplet actually consists of six components shown in Fig. 3 of Dere et al. (1983). The unblended 1560.31 Å component is usually weak and is not used in our map construction, while the other five components form two blended profiles at 1560.7 Å (composed of 1560.68 Å and 1560.71 Å) and at 1561.4 Å (composed of 1561.34 Å and 1561.44 Å). In addition, the Dopplershifts determined from the two observed profiles tend to differ because the C I lines are optically thick. Therefore, we are not certain that our first-moment C I Dopplershift determinations actually represent true bulk flows in the chromosphere. Nevertheless, they are the only velocity indicators in hand, and we are also studying Dopplershifts here of relatively large magnitude.

Locations for which the first moment indicates Dopplershifts in excess of 25 km s^{-1} have been set to this limiting value in our map construction. Locations where the C I intensities do not allow for accurate determination of the line profile are left dark. This occurs typically because of weak emission, but occasionally because of film saturation from

exceptionally bright emission.

2.3. Co-registration of images and maps

The spectrograph slit is visible on the spectroheliograph images, so that its position at the mid-moment of each spectroheliograph exposure could be determined and the C I maps co-registered with the 1600 Å images. The final maps and images have been digitized at 0.5 arcsec pixel size. Their co-registration can be checked by direct frame comparison using an image display system. We estimate the registration to be accurate to three pixels, or 1.5 arcsec.

A subfield of 150×87 arcsec^2 size has been selected from the complete 920×107 arcsec^2 map for more detailed analysis described below. It avoids larger-scale image imperfections in the C I velocity map (fiducial wire positions, dust on the slit, and extended areas where the C I intensity did not allow reliable velocity determination), and is covered by all seven co-aligned 1600 Å images. Its center has solar position angle $\mu = 0.836$. A smaller sub-area of 50×50 arcsec^2 is also used below.

3. Results

We search for correspondence between internetwork bright points in the 1600 Å images and sites of chromospheric jets on the C I velocity map. The input data are illustrated in Fig. 1 in the form of three co-aligned panels, respectively a part of the 1600 Å image taken at $t = 221$ s, the corresponding part of the C I intensity map, and the corresponding part of the C I velocity map. The agreement in bright network patterning between the 1600 Å image (top) and the C I intensity map (middle) is excellent. Sites of large upward (blue) and downward (red) motion in the C I Dopplershift map are predominantly located in the internetwork regions. Within these, large-Dopplershift sites appear to be randomly distributed.

For a closer look, we show in Fig. 2 the result of summing the seven individual 1600 Å images for the 150×87 arcsec^2 subfield. This area lies just left of the fiducial line in the middle of the top panel of Fig. 1. The long-lived network features are enhanced in this 160 s summation, whereas the rapidly varying internetwork brightness features are suppressed. In addition, Fig. 2 displays the positions of "blue jets" superposed as green pixels. Blue jets are here defined as locations with C I blueshift in the range $15 - 25$ km s^{-1}. Dere et al. (1983) specified a velocity range of $10 - 20$ km s^{-1} for chromospheric jets, but

after examining several trial velocity ranges, we settled on $15 - 25$ km s^{-1} because this range preserves jets as relatively point-like features, results in somewhat less crowded area coverage, gives a larger degree of confidence in the velocities as being physically meaningful, and includes the strongest and most obvious examples of chromospheric jets. In addition, we only look at blueshifts although Dere et al. (1983) also described a few redshifted features as chromospheric jets. Figure 2 confirms that blue jets are generally found in internetwork regions (dark red), avoiding the chromospheric network (bright)—although there are exceptions, some blue jets being located within the bright elements of the network. The distribution of blue jet locations over the internetwork regions again seems random, perhaps with some meso-scale clustering.

The C I velocity map is actually an upwards rolling scan, from bottom to top in the lower panel of Fig. 1, sampling the chromospheric velocity field in time-dependent fashion. Each horizontal pixel row was produced from one spectrogram, the next higher row from the subsequent spectrogram, etc. In contrast, the 1600 Å spectroheliograph frames are true images, covering the entire field at once during exposure. Thus, the question we may investigate is whether, at the site of a chromospheric jet that is observed only at the single moment when the spectrograph rastering sampled that location, a concurrent co-spatial internetwork bright point occurs in the 1600 Å images, possibly with some phase delay in temporal development. The scenario of Rutten & Uitenbroek (1991b) suggests that a bright point should develop a few minutes after the initial upward-moving chromospheric jet. The data permit searching for such a correlation with delays up to 174 s, which is the interval between the moment at which the slit rastering started (186 s after launch, bottom line in C I panels of Fig. 1) and the moment of exposure of the last 1600 Å image (360 s after launch).

We first searched for easy-to-note correspondence by visually comparing, on an image display monitor, the Dopplershift map with a movie rendition of the 1600 Å images. After noting the site of a blue jet, we watched the temporal development of the 1600 Å brightness at this location. Doing so for a number of jet sites, we did not note any directly obvious relationship between blue jet locations and 1600 Å bright points, also not when allowing for temporal phase differences of either sign.

Figure 3 enables the reader to simulate such direct inspection. It displays a yet smaller subfield of 50×50 arcsec^2; the larger scale is chosen to keep a a particular jet location easily identifiable between the seven images while the area is yet large enough to contain several network cells. This subfield lies to the lower right in the lefthand half of Fig. 2. The superposed green pixels again mark $15 - 25$ km s^{-1} blueshifts; they are the same for each image. The subfield was scanned bottom to top by the slit spectrograph from $t = 200$ to

$t = 240\,\mathrm{s}$ after launch. Therefore, the upper left image displays 1600 Å brightness at the moment when the jets near the bottom were sampled, while the lower left image was taken simultaneous with the jet sampling near the top of the field; the seven-image sequence covers possible phase lags from $-41\,\mathrm{s}$ to $+160\,\mathrm{s}$.

Inspection shows no direct relationship between blue jets and 1600 Å bright points. A few jets lie in the bright area just above the center of the field, but this is part of the network as is obvious from Fig. 2. If anything, there seems not to be coincidence between jets and above-average 1600 Å brightness, but rather with below-average 1600 Å darkness at a phase lag of about 20 s: the non-network green pixels overlying the bottom of the $t = 221\,\mathrm{s}$ image, the middle of the $t = 242\,\mathrm{s}$ image and the top of the $t = 274\,\mathrm{s}$ image seem to preferentially lie in dark areas.

In order to perform a more quantitative search for relationships between chromospheric jets and 1600 Å bright points, we now examine the 1600 Å brightness characteristics applying a separation between blue jet locations (sites with C I blueshifted over $15 - 25$ km s^{-1} at the moment of Dopplershift sampling by the spectrograph) and the remaining areas, including network. We call these the blue and the non-blue areas, respectively. The area statistics are shown in Fig. 4 which displays the Dopplershift distribution for the 150×87 arcsec^2 subfield in the form of a histogram with 5 km s^{-1} bins, normalized such that the pixels for which the velocity could not be measured are not included. Approximately 14% of this subfield consists of blue areas (the two leftmost columns of the histogram), whereas the corresponding redshift bins on the right contain only 5% of the total. This difference illustrates the preponderance of blue over red jets in Fig. 1, as already noted by Dere et al. (1983).

Figure 5 shows the spatially averaged brightness temperature of each 1600 Å image, split between blue and non-blue areas (solid and dashed curves). Since the average intensity of each full-field image was set equal to $150\,\mathrm{erg\,cm^{-2}\,s^{-1}\,\AA^{-1}\ sr^{-1}}$, the slight variations in average temperature reflect small differences in the intensity distribution between the full-field and subfield images, and also yet smaller differences between the blue versus the non-blue distributions per image. The average temperature is higher in the non-blue area which includes the bright network; blue areas occur predominantly in cell centers.

The symbols in the lower half of Fig. 5 measure corresponding rms variations. For the blue and non-blue areas of each image, respectively, they specify the rms deviation of the brightness temperature per pixel from the time-averaged value of that pixel plotted in Fig. 2. These spatial rms deviations are very similar for the blue and non-blue areas; they measure approximately 25 K with a slight excess for the blue areas (asterisks).

In Fig. 6 we show the temporal development of the average brightness temperature for seven horizontal strips, each measuring 150×12.5 arcsec^2, which together cover the 150×87 arcsec^2 subfield. These were consecutively sampled by the spectrograph slit, lengthwise from bottom to top. Each of the seven curves is shifted in relative time so that the moment at which the slit sampled the middle of each strip occurs at $t = 0$ s. Thus, the seven strips are lined up in common phase with respect to the Dopplershift measurement, while each individual curve covers a different temporal range around that moment. This display serves to search for a systematic phase advance or phase delay in the occurrence of bright points at sites of chromospheric jets. Each curve plots the difference between the brightness temperature averaged per image over the strip and the time-averaged mean of that strip in all seven images, again split between blue and non-blue pixels. Across a strip, the Dopplershift measurements all occur within about 20 s, a period shorter than the one-minute lifetime of bright points and the 40 s duration of jets measured by Dere et al. (1983). On the other hand, the strips are sufficiently long that small-scale brightness variations from film noise and from actual solar brightness modulation such as the 250 s brightness oscillation with 50 K average amplitude reported by Cook & Ewing (1991) tend to cancel out when averaged over a full strip. But if 1600 Å bright points appear at jet sites with a characteristic phase shift prior to or after the jet occurs, they should not cancel out but add constructively and so produce an increase in the average brightness temperature at jet sites at that characteristic phase shift. An average brightness peak should then be present at a given time interval before or after $t = 0$ in Fig. 6 for blue areas, while such a peak should not be present in the non-blue data.

How large should such a differential peak be? An average network bright point is approximately 300 K brighter than the average brightness temperature (Cook & Ewing 1990). The internetwork bright points are typically not this bright but still produce a signal of order $50 - 100$ K (Foing & Bonnet 1984), well above the average background variation. Thus, a systematic brightening of order 100 K in the blue-area temporal evolution relative to the non-blue evolution in Fig. 6 would represent evidence for bright-point emission at that particular phase delay relative to the jet occurrence. However, the curves in Fig. 6 show modulation due to differences between the normalization of the large-field original images and the strip-wise averaging, but no significant difference between the blue and non-blue areas. Their brightness temperatures vary in step, with only the slight (order 10 K) deficits in blue areas also seen in Fig. 5. There is no sign of an systematic blue over non-blue brightening of order 100 K at any phase shift. In Fig. 7 we show a similar plot for the average rms deviation in brightness temperature per strip. Again, we find no systematic difference between blue or non-blue areas.

4. Discussion

We have been unable to find any systematic correlation between the sites of 1600 Å internetwork bright points and sites of blue jets, also not when allowing for phase delays between the two phenomena as long as three minutes. Also, we have not found any systematic difference in the temporal evolution of the average brightness or its average rms fluctuation between blueshifted areas and the remaining non-blueshifted area. Thus, we find no clear evidence for a direct relationship between internetwork bright points and jets as suggested by Rutten & Uitenbroek (1991a, 1991b). A more intricate and indirect relationship, derived from statistical analysis of the same data, is described by Hoekzema et al. (1996).

Our analysis above does not rule out a direct correlation for phase delays above three minutes, which may occur in Rutten & Uitenbroek's scenario if the wake oscillation requires multiple cycles before shocks of sufficient strength develop. Unfortunately, such ranges of temporal development cannot be investigated from a sounding rocket flight.

A desirable option for further study is to employ groundbased Ca II K data over a longer time span, in order to compare Ca II K_{2V} bright points with rocket maps of chromospheric Dopplershifts as used here. This may also directly confirm (or disprove) the identity of Ca II K_{2V} bright points and 1600 Å bright points, but requires a HRTS rocket flight with simultaneous high-quality groundbased coverage in Ca II. So far this has not been successfully accomplished. Another option, obviously, is to obtain space observations from platforms in orbit. More generally, such studies of chromospheric internetwork dynamics may supply a valuable probe of the magnetic canopies which are thought to occur over the interiors of supergranulation cells.

J.W. Cook's work was supported by NASA under DPR W–14,541 and by the Office of Naval Research. N.M. Hoekzema's research was supported by the Netherlands Foundation for Research in Astronomy (NFRA) with financial aid from the Netherlands Organization for Scientific Research (NWO).

References

Bartoe, J.-D. F., Brueckner, G. E. 1975, J. Opt. Soc. Am., 65, 13

Bonnet, R. M., Bruner, M., Acton, L. W., Brown, W. A., Decaudin, M., Foing, B. 1982, A&A, 111, 125

Brueckner, G. E., Bartoe, J.-D. F. 1983, ApJ, 272, 329

Brueckner, G. E., Bartoe, J.-D. F., VanHoosier, M. E. 1978, in E. Hansen, S. Schaffner (eds.), Procs. OSO-8 Workshop, Univ. Colorado, Boulder, p. 380

Carlsson, M., Stein, R. F. 1994, in M. Carlsson (ed.), Chromospheric Dynamics, Proc. Miniworkshop, Inst. Theor. Astrophys., Oslo, p. 47

Cook, J. W., Brueckner, G. E., Bartoe, J.-D. F. 1983, ApJ, 270, L89

Cook, J. W., Brueckner, G. E., VanHoosier, M. E. 1980, J. Geophys. Res. A5, 85, 2257

Cook, J. W., Ewing, J. A. 1990, ApJ, 355, 719

Cook, J. W., Ewing, J. A. 1991, ApJ, 371, 804

Dere, K. P. 1994, Space Sci. Rev, 70, 21

Dere, K. P., Bartoe, J.-D. F., Brueckner, G. E. 1983, ApJ, 267, L65

Dere, K. P., Bartoe, J.-D. F., Brueckner, G. E. 1984, ApJ, 281, 870

Dere, K. P., Bartoe, J.-D. F., Brueckner, G. E. 1986, ApJ, 305, 947

Dere, K. P., Bartoe, J.-D. F., Brueckner, G. E., Ewing, J., Lund, P. 1991, J. Geophys. Res. A6, 96, 9399

Dere, K. P., Bartoe, J.-D. F., Brueckner, G. E., Recely, F. 1989, ApJ, 345, L95

Foing, B., Bonnet, R. M. 1984, ApJ, 279, 848

Hoekzema, N. M., Rutten, R. J., Cook, J. W. 1996, ApJ, submitted

Rutten, R. J. 1994, in M. Carlsson (ed.), Chromospheric Dynamics, Proc. Miniworkshop, Inst. Theor. Astrophys., Oslo, p. 25

Rutten, R. J. 1995, in J. T. Hoeksema, V. Domingo, B. Fleck, B. Battrick (eds.), Helioseismology, Proc. Fourth SOHO Workshop, ESA SP–376 Vol. 1, ESA Publ. Div., ESTEC, Noordwijk, p. 151

Rutten, R. J., Uitenbroek, H. 1991a, Solar Phys., 134, 15

Rutten, R. J., Uitenbroek, H. 1991b, in P. Ulmschneider, E. R. Priest, R. Rosner (eds.), Mechanisms of Chromospheric and Coronal Heating, Proc. Heidelberg Conf., Springer Verlag, Berlin, p. 48

Samain, D. 1979, A&A, 74, 225

Sivaraman, K. R., Livingston, W. C. 1982, Solar Phys., 80, 227

Vernazza, J. E., Avrett, E. H., Loeser, R. 1981, ApJS, 45, 635

This manuscript was prepared with the AAS LaTeX macros v3.0.

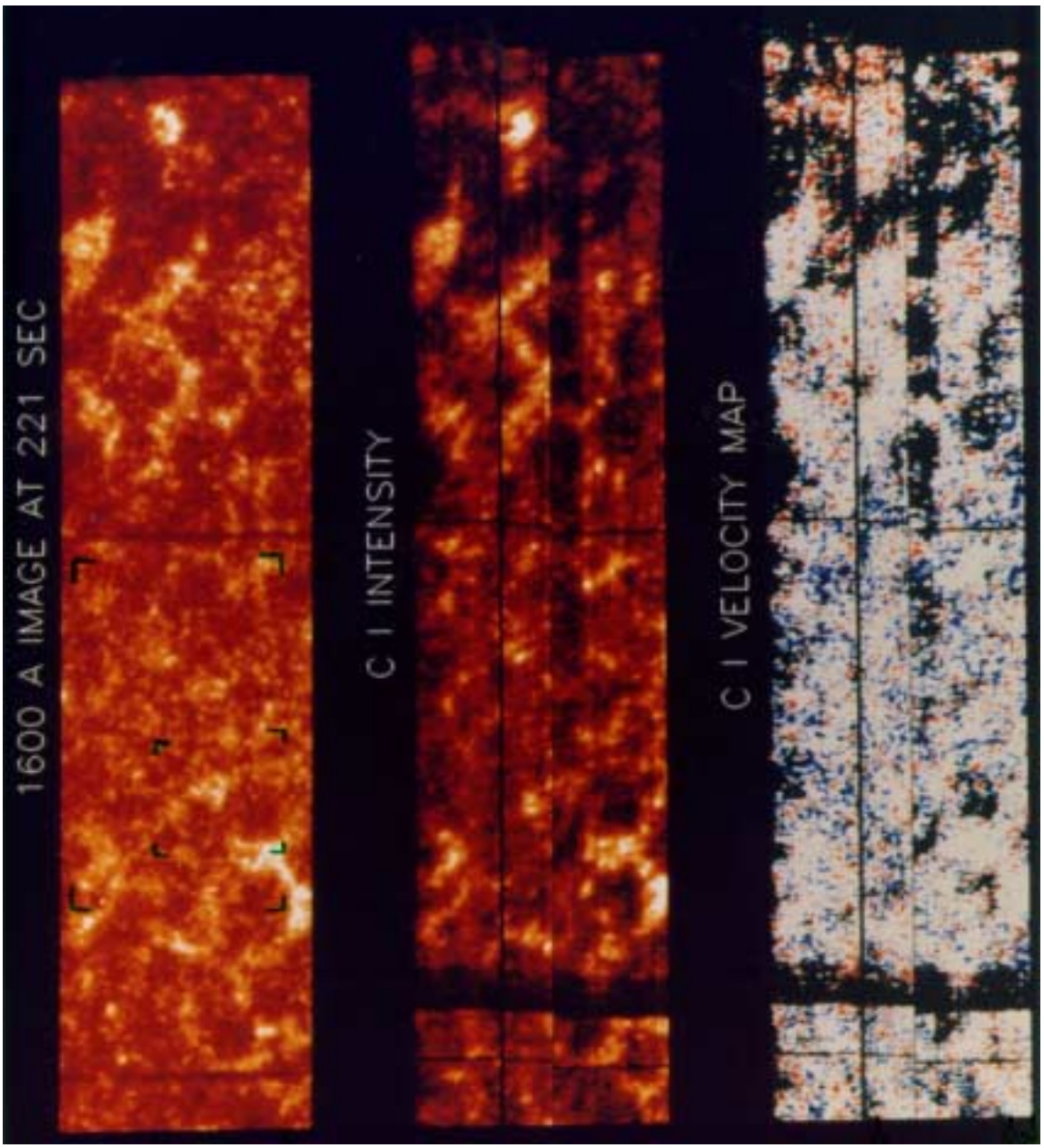

Fig. 1.— A subset of HRTS VI data. Top: part of the 1600 Å spectroheliogram taken at $t = 221$ s after launch. Middle: corresponding part of the C I intensity map produced from three spectrum rasters taken with the slit spectrograph. Bottom: corresponding part of the C I Doppler map. Blue indicates blueshift, red indicates redshift, black areas are locations where no reliable Dopplershift could be obtained from the C I line profiles. The long dimension is about half of the full slit length of 920 arcsec. The slit was stepped from bottom to top over 107 arcsec in three raster sequences with steps of 2 arcsec, 1 arcsec and 2 arcsec, respectively, covering a period of 174 s starting at $t = 186$ s after launch. The dark horizontal lines are gaps between raster sequences, the thin vertical lines are from fiducial wires, the irregular band near the center of the two C I maps is probably due to a dust flake on the spectrograph slit.

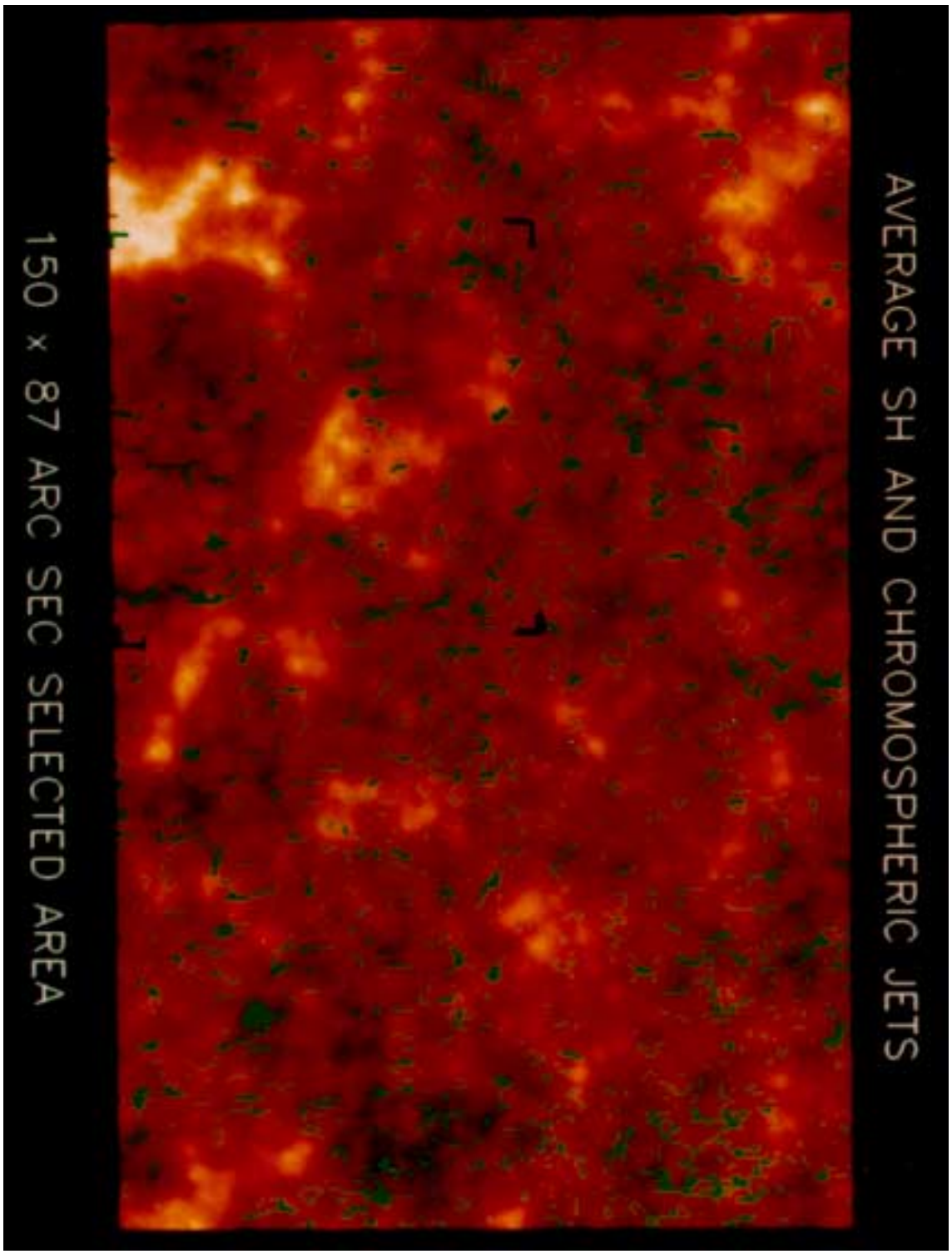

Fig. 2.— Temporally averaged 1600 Å brightness for the 150×87 arcsec^2 subfield, constructed from seven 1600 Å spectroheliograph images. This area lies in the left half of the 1600 Å image in the top panel of Fig. 1. The locations of blue jets (pixels with $15 - 25$ km s^{-1} blueshift at the moment of sampling by the spectrograph) are superposed in green.

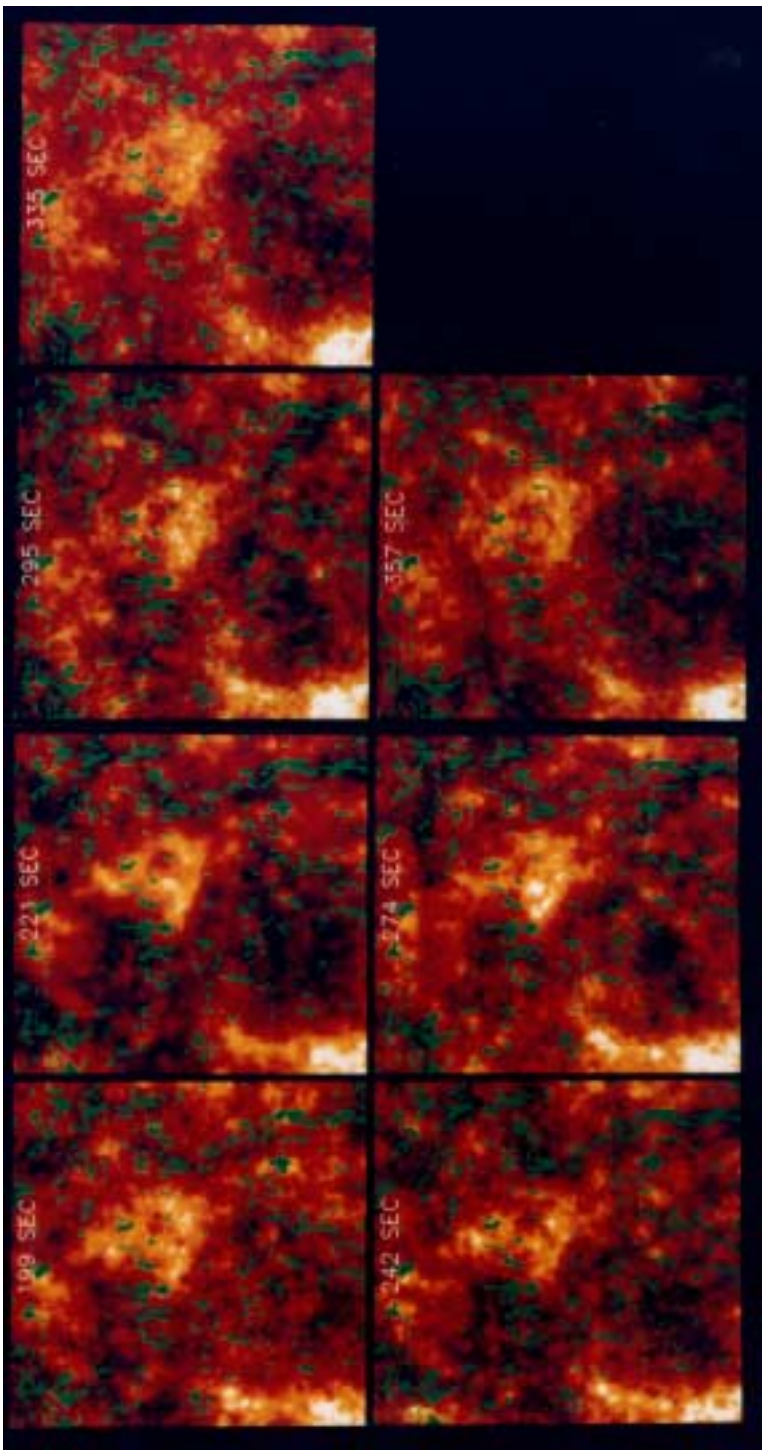

Fig. 3.— The 50×50 arcsec^2 subfield in the sequence of seven 1600 Å images. The subfield lies to the lower left from the center of Fig. 2. The moments of exposure (seconds after launch) are indicated. The green pixels again identify blue jet locations as sampled by the spectrograph. The spectrograph slit scanned this subfield from bottom to top during $t = 200\,\mathrm{s}$ to $t = 240\,\mathrm{s}$.

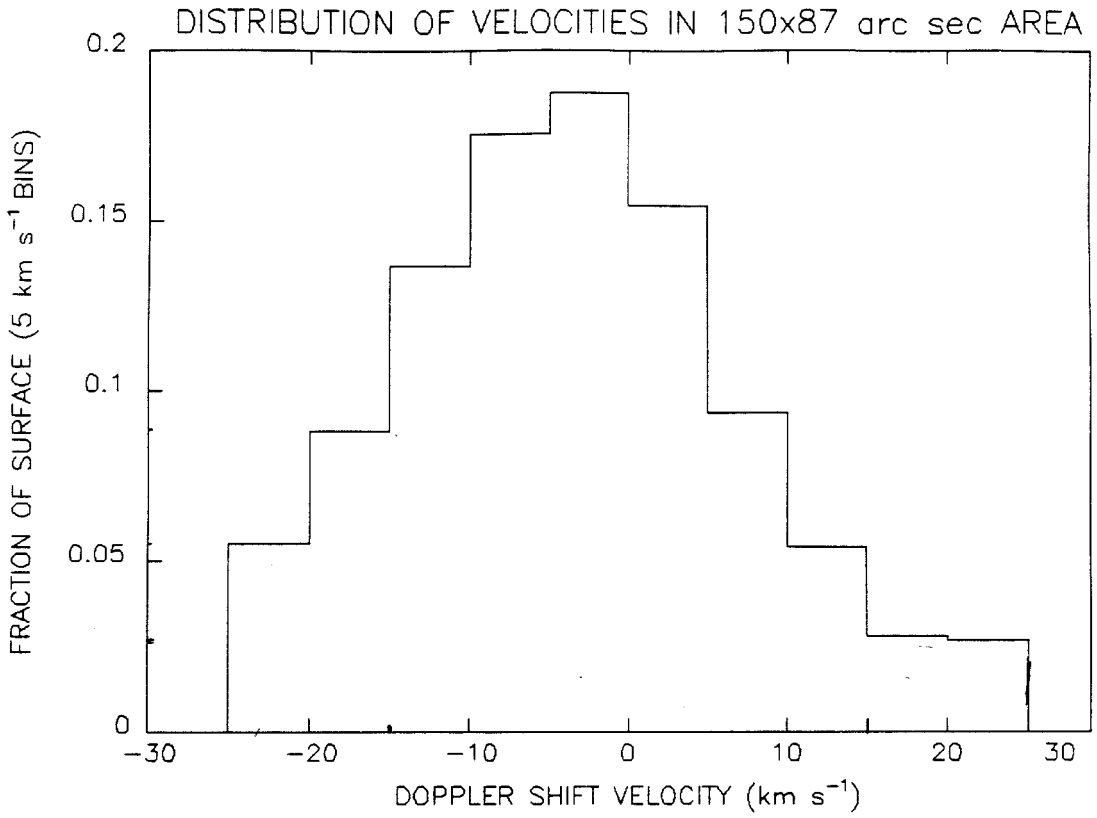

Fig. 4.— Histogram distribution of velocities within the 150×87 arcsec^2 subfield. Blue jets ($15 - 25$ km s^{-1} blueshift) cover 14% of the surface.

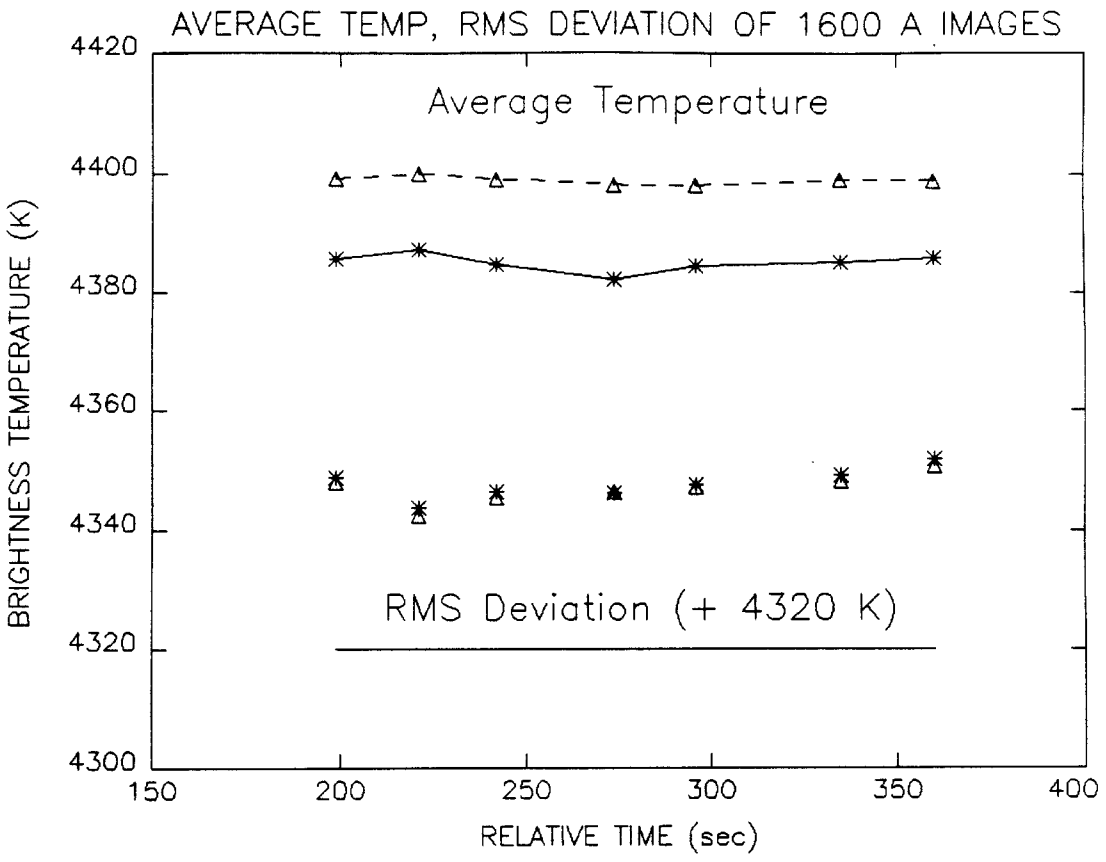

Fig. 5.— Upper symbols and curves: spatially averaged brightness temperature for the 150×87 arcsec^2 subfield of each of the seven 1600 Å images, split between blue ($*$) and non-blue (Δ) areas. Lower symbols: blue and non-blue spatial rms deviations from average, at an offset of 4320 K above zero.

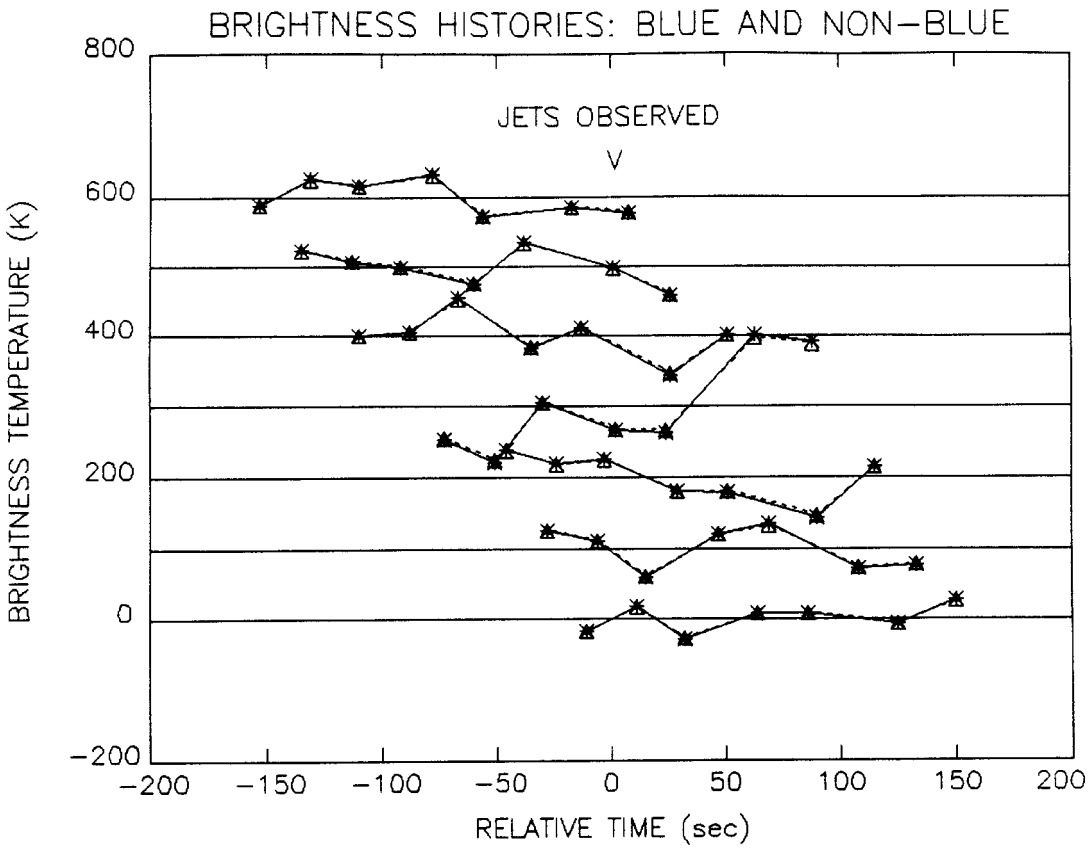

Fig. 6.— Brightness temperature evolution for seven 12.5 arcsec wide strips across the 150×87 arcsec^2 subfield, each on a shifted temporal axis so that $t = 0$ corresponds to the moment of mid-strip sampling by the spectrograph slit for all curves. The symbols specify the average difference in brightness temperature between each strip and its seven-image average, respectively for blue areas (asterisks) and non-blue areas (triangles). The curves are displaced vertically from each other by 100 K.

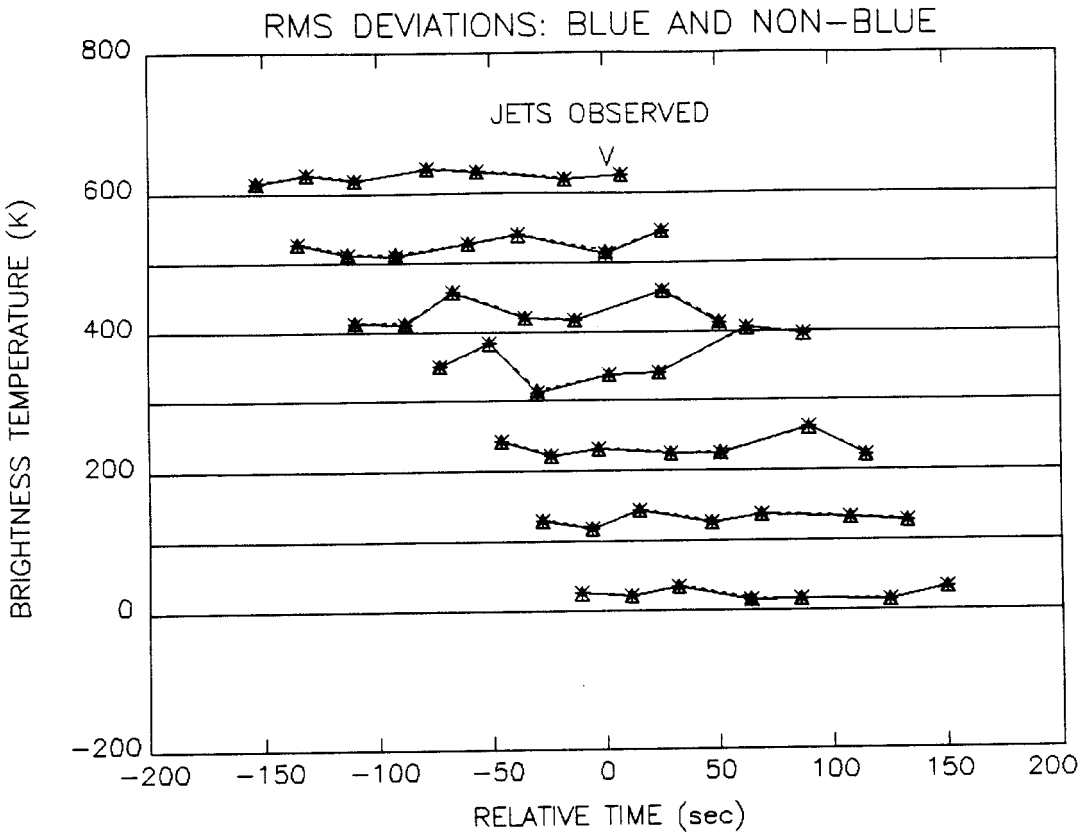

Fig. 7.— As Fig. 6 for rms brightness variation.